XL CILAMCE
IBERO-LATIN AMERICAN CONGRESS ON COMPUTATIONAL METHODS IN ENGINEERING
NOVEMBER 11-14, 2019
Praiamar Natal Hotel & Convention
Natal, RN-BRAZIL

A 2D BOUNDARY ELEMENT FORMULATION FOR POLLUTANT DISPERSION ON THE ATMOSPHERIC BOUNDARY LAYER

Luiz F. Bez
Rogério J. Marczak
Marco T. M. B. de Vilhena
luiz.bez@ufrgs.br
rato@mecanica.ufrgs.br
mtmbvilhena@gmail.com
Universidade Federal do Rio Grande do Sul - UFRGS
Programa de Pós Graduação em Engenharia Mecânica - PROMEC
Sarmento Leite street, number 425, 2nd floor, 90050170 Porto Alegre, RS, Brazil

Abstract. This paper presents a boundary element formulation for 2D, steady-state advection-diffusion problems with a variable velocity field and punctual source terms. The boundary and the variables are discretized with continuous linear elements. The domain effects are computed with discontinuous linear cells. The model shows good agreement with analytical results for variable velocity fields. Four cases are presented with wind configuration typical of the atmospheric boundary layer - a combination of wind power classes 1 and 4 for mean velocity, and open flat terrain and suburban areas for roughness. The response of a unitary point source is analyzed and compared for each case.

Keywords: Boundary element method, Pollutant dispersion, Atmospheric boundary layer.

1 Introduction

The knowledge of the pollutant dispersion simulation in the planetary boundary layer (PBL) for a point source is relevant not only to control the impact of the environmental damage of an accidental event but also to project the site of an industrial complex in order of minimize such event. Furthermore from the Green Function Theory the solution of an arbitrary pollutant source can be straightly obtained from the knowledge of the solution for a point source.

The advection-diffusion equations that models this phenomenon, if solved via the traditional numerical domain methods, usually requires fine meshing discretization for problems with high velocity field and point sources, which demands a significant computational time for the numerical simulations, (Roache [1]).

We must notice that the analytical methods can be applied to problems with regular domains but not for realistic domains like the ones with complex topography terrain.

One alternative is to employ analytical solutions in order to analyze a simplified version of the problem. This, however, is only practical for very specific circumstances and results on a loss in solution quality when applied to realistic situations (Cunha and Costa [2]).

Ikeuchi and Onishi [3] showed that the boundary element method (BEM) can be used as an alternative for decreasing the problem size and maintaining solution quality. Also, the upwind effect of the mean velocity field is accounted for on the fundamental solution, allowing for the mesh used to be coarser and the solution numerically more efficient and stable even for very high Péclet numbers (Qiu [4]). The BEM solution can account for velocity fields high deviations from the mean with domain integration, as shown by Wrobel and de Figueiredo [5]. However, according to Cunha and Costa [2], BEM applications to advction-diffusion problems are scarce and to the best of our knowledge there is no application to problems in the PBL.

In this paper we present a BEM formulation applied to solve the advection-diffusion problem for a point source in a rectangular domain for some PBL typical flows, al well we also report numerical simulation and comparisons against literature results.

2 Mathematical Formulation

The pollutant transport, in a Reynolds Average sense, can be described as Eq. (1), taking into account advective, diffusive, and linear reaction effects.

$$\vec{v} \cdot \nabla\phi - d\,\nabla^2\phi + k\,\phi = f \tag{1}$$

where $\phi = \phi(\vec{x})$ is the time average pollutant concentration, $\vec{v} = \vec{v}(\vec{x})$ is the velocity field, d is the turbulent diffusivity, k is the rate os consumption of ϕ, and $f = f(\vec{x})$ is the source term. Eq. (1) implies an incompressible velocity field.

The part of this differential problem with constant coefficients has a fundamental solution associated to it, which we will call u_i^*. The subindex i refers to the application point of the Dirac's delta. u_i^* is given by the solution to:

$$\vec{v}_m \cdot \nabla u_i^* + d\,\nabla^2 u_i^* - k\,u_i^* = -\delta(\vec{x}_i) \tag{2}$$

in infinite domain with evanescent primal and dual variables when the distance from $\vec{x}_i$ tends to infinity. In Eq. (2) $\vec{v}_m$ is the spatial mean of the velocity field. The solution to Eq. (2) is given by:

$$u_i^* = \frac{1}{2\pi d} \exp\left(-\frac{\vec{v}_m \cdot \vec{r}}{2d}\right) K_0\left(\mu r\right) \tag{3}$$

where K_ν is the modified Bessel function of the second kind and order ν, $\vec{r}$ is the distance from $\vec{x}_i$, and μ is given by:

$$\mu = \sqrt{\left(\frac{v_m}{2d}\right)^2 + \frac{k}{d}} \tag{4}$$

The derivative of the fundamental solution in a direction n is:

$$\frac{\partial u_i^*}{\partial n} = -\frac{1}{2\pi d}\exp\left(-\frac{\vec{v}_m \cdot \vec{r}}{2d}\right)\left[\mu K_1(\mu r)\frac{\partial r}{\partial n} + \frac{\vec{v}_m \cdot \vec{r}}{2d}K_0(\mu r)\right] \tag{5}$$

Equation (1) can be rewritten in its integral form, as shown by Wrobel [5]:

$$c(\vec{x}_i)\phi(\vec{x}_i) + \int_\Gamma \phi\,(v_n\,u_i^* + d\,q_i^*)\,\mathrm{d}\Gamma - \int_\Gamma q_n\,d\,u_i^*\mathrm{d}\Gamma = \int_\Omega \phi\,(u_i^*\,\nabla\cdot\vec{v}_p + \vec{v}_p\cdot\nabla u_i^*)\,\mathrm{d}\Omega + \int_\Omega f\,u_i^*\mathrm{d}\Omega \tag{6}$$

where c is a coefficient that depends on the location of $\vec{x}_i$, being 1 if it is inside the domain, zero if outside and depending on the internal angle of Γ at $\vec{x}_i$ if it is at the boundary (Brebbia, Telles and Wrobel [6]); v_n is the velocity outward normal to the boundary and $\vec{v}_p$ is the difference between the velocity and the mean velocity. q_i^* is given by $u_i^* \cdot \vec{n}$, and q_n is the normal diffusive flux given by $\partial\phi/\partial\vec{n}$.

Equation (6) as written is used in one of the benchmarks, but it can be simplified for incompressible flows such as those in the PBL, resulting in:

$$c(\vec{x}_i)\phi(\vec{x}_i) + \int_\Gamma \phi\,(v_n\,u_i^* + d\,q_i^*)\,\mathrm{d}\Gamma - \int_\Gamma q_n\,d\,u_i^*\mathrm{d}\Gamma = \int_\Omega \phi\,\vec{v}_p\cdot\nabla u_i^*\,\mathrm{d}\Omega + \int_\Omega f\,u_i^*\mathrm{d}\Omega \tag{7}$$

The domain integral with respect to the source term given by f will receive a analytical treatment. In this work we consider f as being a series of point sources modeled as Dirac delta functions:

$$f = \sum_{k=1}^{N_s} Q_k\,\delta(\vec{x}_k) \tag{8}$$

where N_s is the number of sources, Q_k is the strength of the source k, and $\vec{x}_k$ is the position of source k. Using Eq. (8) we rewrite the domain integral:

$$\int_\Omega f\,u_i^*\mathrm{d}\Omega = \sum_{k=1}^{N_s} Q_k\,u_i^*(\vec{x}_k) \tag{9}$$

3 Numerical Implementation

3.1 Discretization and Matrix Equations

Equation (7) was discretized and solved numerically. The variables ϕ and q_n at the boundary, and the boundary itself, were interpolated using 1D linear finite elements. The elements were continuous

everywhere except at points where the boundary was not smooth or the boundary conditions had a discontinuity, where they were formulated as discontinuous.

The domain integrals were computed using discontinuous linear cells. It is worth remembering that the BEM formulation uses domain integrals for computing domain effects, and not for building a solution.

A matrix system was created by applying Eq. (7) at collocation points coinciding with the nodes used in the interpolation of the boundary. This generates the matrix Eq. (10). We need the concentration values for the domain cells, and for that we apply Eq. (7) at each cell node, generating Eq. (11).

$$H^b_{ij}\phi_j - G^b_{ij}q_{n,j} - B^b_{il}\phi_l = b_i \tag{10}$$

$$H^d_{ij}\phi_j - G^d_{ij}q_{n,j} - B^d_{il}\phi_l = b_i \tag{11}$$

where the subscript i corresponds to a collocation point, j corresponds to a boundary node, l corresponds to a domain cell node. The superscript b corresponds to a collocation point belonging to the boundary, while d corresponds to one belonging to the domain. b_i is the computation of Eq. (9).

In well posed problems we know either the primal or the dual variable in each portion of the boundary, with at least a portion of it with the primal variable known. For each boundary node we know either ϕ_j or $q_{n,j}$, so in order to assemble the final linear system we shuffle the corresponding columns of H and G, forming a matrix A for the unknown values χ and a vector a resulting form the matrix multiplication of the known values. The final system is given by:

$$\begin{bmatrix} A^b_{ij} & -B^b_{il} \\ A^d_{ij} & -B^d_{il} \end{bmatrix} \begin{bmatrix} \chi^b_j \\ \phi_l \end{bmatrix} = \begin{bmatrix} (b^b_i + a^b_i) \\ (b^d_i + a^d_i) \end{bmatrix} \tag{12}$$

3.2 Numerical Integration

The boundary and domain integrals used to assemble the matrix system were solved with the Gauss-Legendre quadrature if they did not contain a singularity. If they did contain a singularity, special treatment is required.

Qiu [4] showed the asymptotic behavior of the singularities present on the 2D advection-diffusion-reaction problem. The G matrix has weakly singular kernels to be calculated for its diagonal, the H matrix has a combination of strongly and weakly singular terms in its diagonal, and the B matrix has weakly singular terms. Weakly singular kernels were integrated using a cubic coordinate transformation proposed by Telles [7].

The singular integrals on the H matrix could be solved indirectly, as suggested by Brebbia [8], if there were no reaction term. We chose to integrate directly the diagonal of H. In geometrically linear elements, such as the case of this paper, the strongly singular part of the kernel vanishes and it can be computed by the same scheme used for weakly singular kernels.

3.3 Solution at Interior Points

As mentioned above, the domain cells are used for computing domain effects, and not for building the solution. In effect, usually a small number of cells suffice for the calculation of these effects as shown by Brebbia [8] [6].

In order to analyze results at the interior we can apply Eq. (7) at any domain point that we want, since we already know the primal and dual values at the boundary, and also the necessary values for computing the domain effects. The BEM solution itself is continuous in the domain and is a criterion of the user how many interior points need to be calculated for data analysis.

4 Benchmark Cases

We show the accuracy of the scheme used by solving two cases with analytical solution, one where the velocity varies linearly with x and another where it varies quadratically with y.

4.1 First Case - Linearly Varying Velocity

In this case we solve a problem in a unit square where the velocity in y is zero throughout the domain and the velocity in the x direction can be expressed by:

$$v_x(x) = \ln \frac{\phi_b}{\phi_a} + k\left(x - \frac{1}{2}\right) \tag{13}$$

ϕ_a is the concentration at $x = 0$ and ϕ_b is the concentration at $x = 1$. We have condition of zero diffusive flux on $y = 0$ and $y = 1$, and the diffusion coefficient was held equal to 1. A particular solution to Eq. (1) with this velocity field is:

$$\phi(x) = \phi_a \exp\left[\frac{k}{2}x^2 + \left(\ln \frac{\phi_b}{\phi_a} - \frac{k}{2}\right)x\right] \tag{14}$$

This problem was solved with 40 boundary elements and 10 cells in the x direction, with four different values for k. In this benchmark only we solved Eq. (6) instead of Eq. (7), since the velocity field is compressible. From Eq. (13) we see that the greater the value of k the grater is the variation of the velocity on the domain.

Figure (1) shows a surface plot with the calculated concentration value for this benchmark problem using $k = 4$. Figure (2) shows a comparison between the numerical results for ϕ at the boundary $y = 0$ with the analytical solution. Figure (3) shows a comparison between the numerical results for q_n at the boundary $x = 0$ with the analytical solution. These last results show some spurious oscillations near the corners of the domain that increase with the value of k. They reach 4% deviation with $k = 10$ and they get smaller with finer meshes.

4.2 Second Case - Quadratically Varying Velocity

For this benchmark we solve a problem in a unit square where the velocity in y is zero throughout the domain and the velocity in the x direction can be expressed by:

$$v_x(y) = \frac{(k - C^2)^2}{C}(y - B)^2 \tag{15}$$

where B and C are arbitrary. A particular solution to Eq. (1) with this velocity field is:

$$\phi(x) = \phi_c \exp\left(\frac{\lambda}{2}y^2 - \lambda B y + Cx\right) \tag{16}$$

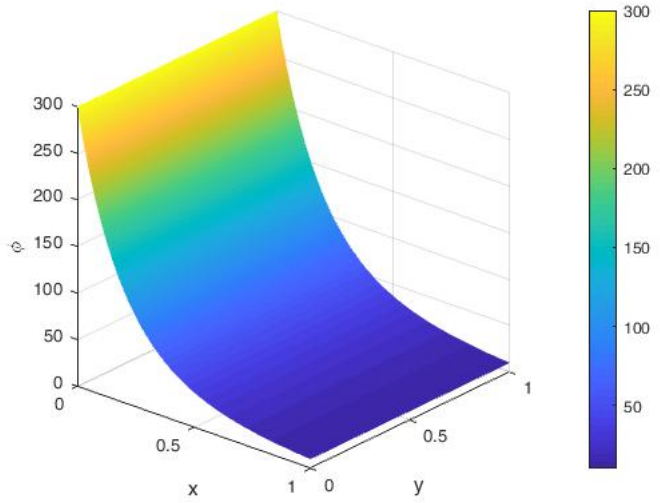

Figure 1. Surface plot for the concentration ϕ of the first benchmark case with $k = 4$.

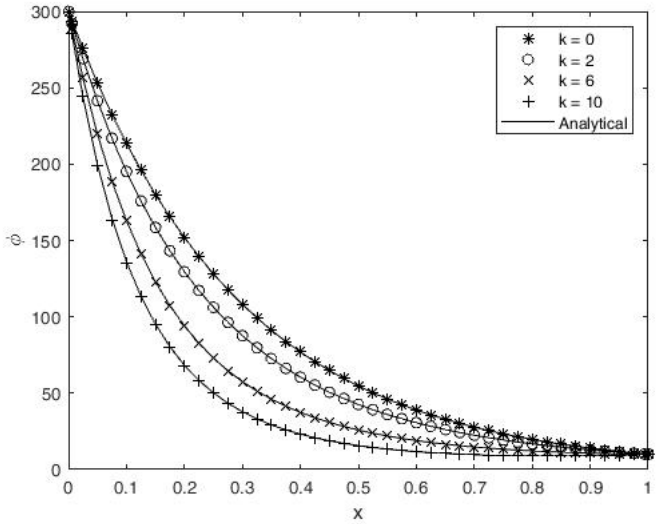

Figure 2. Concentration values along the x direction for different values of the reaction coefficient k. Comparison between numerical and analytical values.

In order to compare the present results with those obtained by Wrobel [5], we choose $d = 1$, $k = 9.724$, $\phi_c = 300$, $B = 0.25$, and $C = -3.4012$. The analytical value for the primal variable was applied at $x = 0$ and $x = 1$ and the analytical value for the dual variable was applied at $y = 0$ and $y = 1$.

This problem was solved with 40 boundary elements and 10 cells in the x direction. The solution is asymmetrical in both the x and y directions.

Figure (4) shows a surface plot with the calculated concentration value for this benchmark problem. Figure (5) shows a comparison between the numerical results for ϕ at the boundaries $y = 0$ and $y = 1$ with the analytical solution. Figure (6) shows a comparison between the numerical results for q_n at the boundaries $x = 0$ and $x = 1$ with the analytical solution. These last results showed again some spurious oscillations near the corners of the domain.

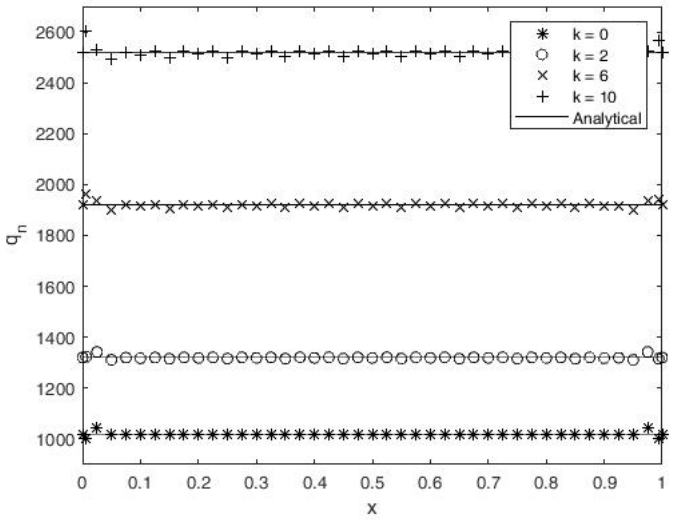

Figure 3. Normal diffusive flux values along the y direction and $x = 0$ for different values of the reaction coefficient k. Comparison between numerical and analytical values.

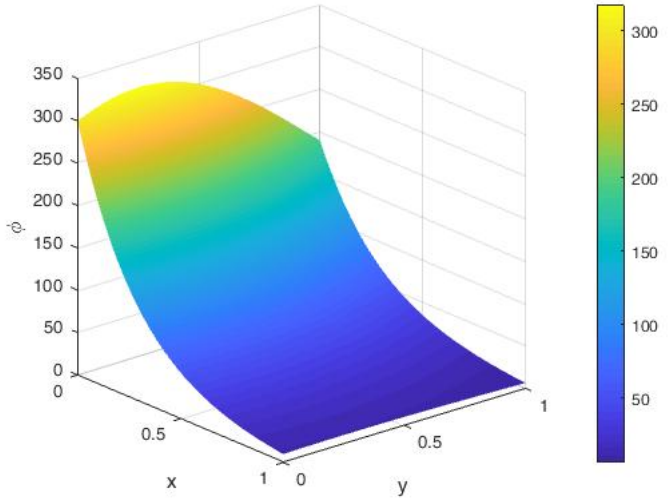

Figure 4. Surface plot for the concentration ϕ of the second benchmark case.

5 Application to Atmospheric Boundary Layer Flows

In this section we will consider a typical atmospheric boundary layer flow for flat terrain and a neutrally stratified PBL, the logarithmic profile:

$$v_x(y) = C \ln\left(\frac{y + y_0}{y_0}\right) \tag{17}$$

where C is the friction velocity divided by the Von Kárman constant and y_0 is a roughness measurement. Four cases will be considered, the combination of two wind power classes and two terrain types. The values for C and y_0, as well as the average wind speed in the first $200m$, are shown at the Table 1.

The wind power classes were defined according to the Wind energy resource atlas of the United States [9] and the terrain roughness values accordingly to the Guide to Meteorological Instruments and

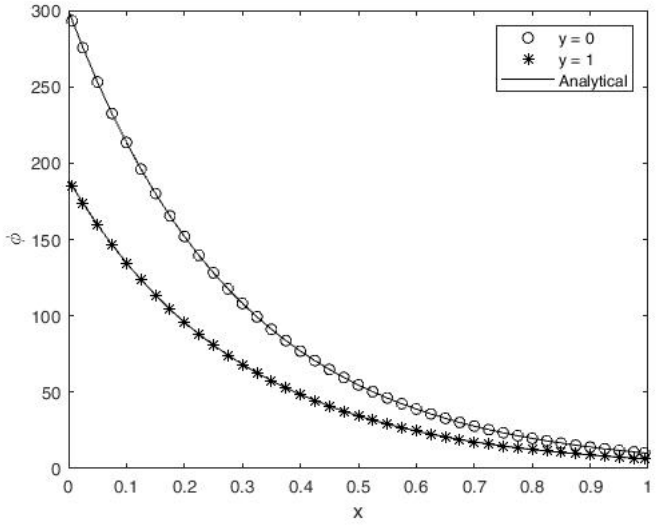

Figure 5. Concentration values along the x direction for the second benchmark case. Comparison between numerical and analytical values.

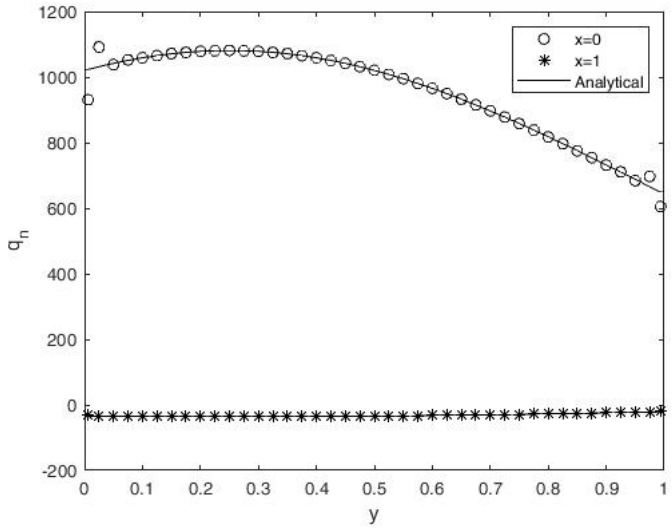

Figure 6. Normal diffusive flux values along the y direction for the second benchmark case. Comparison between numerical and analytical values.

Table 1. Wind profile information.

Case number	Power Class	Terrain	$C(m/s)$	$y_0(m)$	$v_m(m/s)$
I	1	Open field	0.37	0.03	2.91
II	1	Suburb	0.37	1.00	1.61
III	4	Open field	0.90	0.03	7.03
IV	4	Suburb	0.90	1.00	3.90

Methods of Observation [10].

Cases I to IV were solved for a diffusive coefficient of 10 and for $k = 0$, in the domain represented in the Figure 7. We considered air at $x = 0$ without any concentration, and null diffusive flux at the rest

of the boundary. A unitary point source was placed 40 meters above the ground. 120 boundary elements and 50 domain cells were used for the simulations.

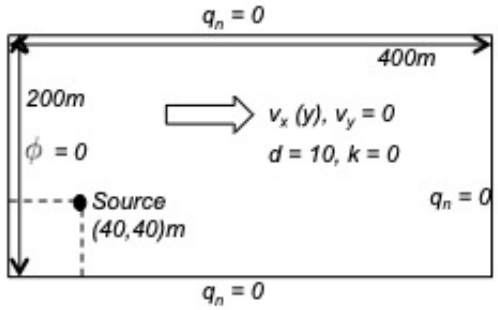

Figure 7. Geometry and boundary condition information.

Figures 8 to 11 show the wind profile and concentration contour plots for the four studied cases. We can observe that the stronger the wind, the smaller are the concentration values and the reach of the plume upwards.

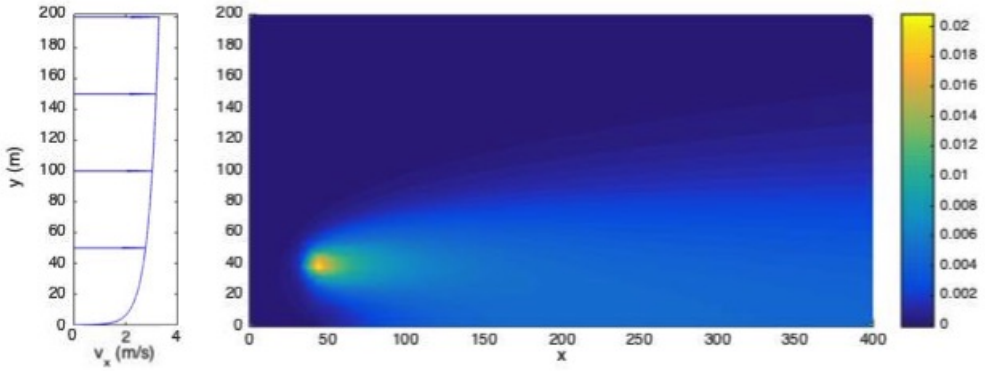

Figure 8. Wind profile and concentration contour plot, case I. Wind power class 1 in a flat open field.

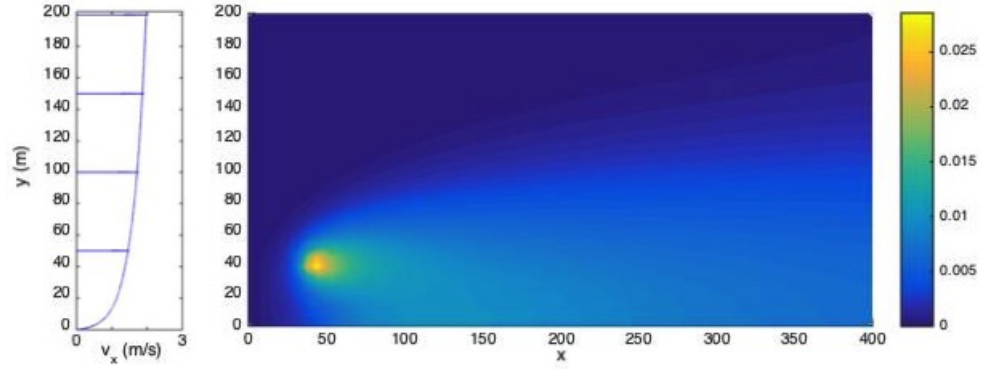

Figure 9. Wind profile and concentration contour plot, case II. Wind power class 1 in a suburban area.

Ne next figures will compare the concentration at three different heights: 10m, 40m, and 70m, for each case studied. In Figure 13 we see the concentration along the x direction at the same height as the source. As expected the concentration falls with the distance.

In Figure 12, at a height of 10m, we see that the concentration behaves somewhat different. In particular, for Case II (wind power class I in a suburban area, the weaker wind studied) the concentration reaches a peak around 80m after the source location. For Case III, with stronger winds, the concentration mounts slowly not appearing to reach a maximum on the simulated domain.

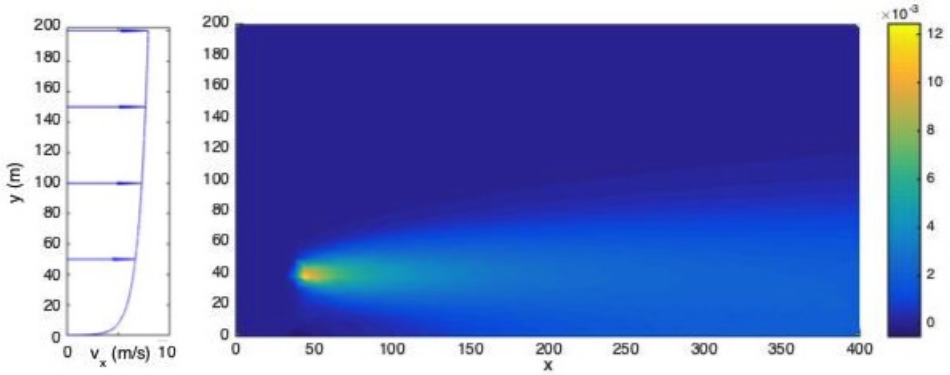

Figure 10. Wind profile and concentration contour plot, case III. Wind power class 4 in a flat open field.

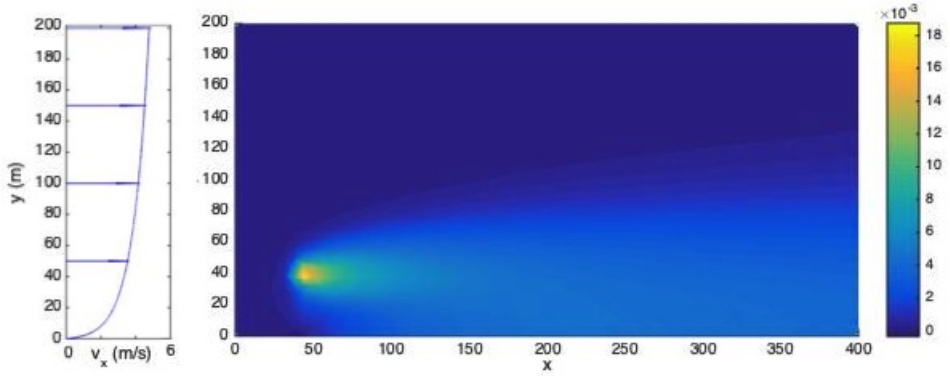

Figure 11. Wind profile and concentration contour plot, case IV. Wind power class 4 in a suburban area.

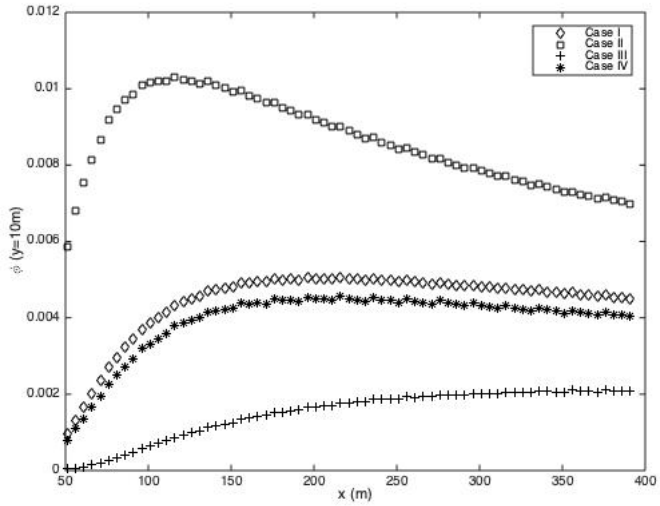

Figure 12. Wind profile and concentration contour plot, case IV. Wind power class 4 in a suburban area.

Figure 13 shows the concentration behavior at the height of the source. As expected, it falls monotonically with the distance, faster the stronger the wind is.

Finally, in Figure 14 we see the concentration at 70m. The changes in concentration at this height are smaller with distance when compared with the other cases, and the absolute value is smaller since the wind is stronger and there is no ground to stop the dispersion.

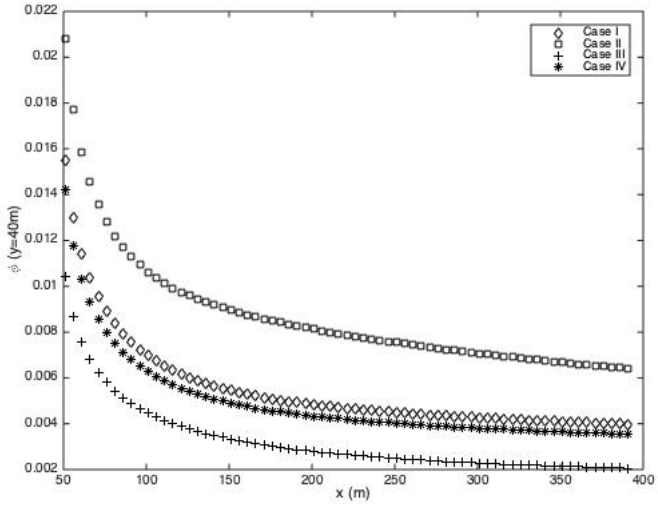

Figure 13. Wind profile and concentration contour plot, case IV. Wind power class 4 in a suburban area.

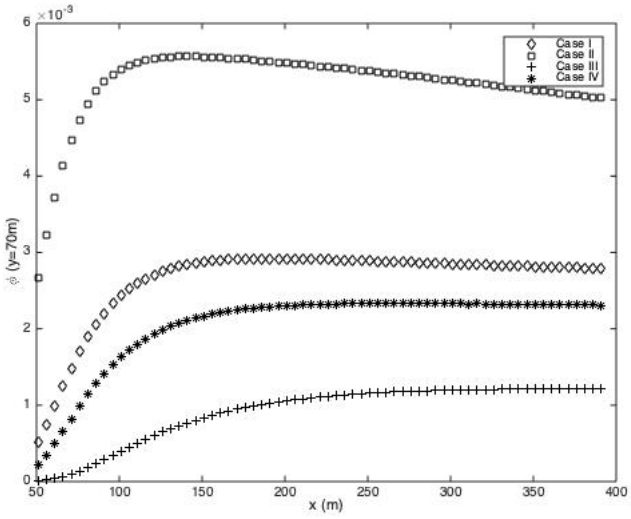

Figure 14. Wind profile and concentration contour plot, case IV. Wind power class 4 in a suburban area.

6 Conclusion

In this work we solved the advection-diffusion equation for pollutant dispersion simulations in the PBL considering a point source in a rectangular domain. To our best knowledge the solution for this kind of problem by the BEM method is not found in the literature.

It is well known that the solution for an arbitrary pollutant source is promptly solved using the Green Function Theory, once the point source solution is known. Taking into account the main feature of the boundary element method which consist in the discretization of the boundary domain, we are confident to affirm that the aforementioned method is robust to solve realistic problems with complex topography terrain. Therefore we shall focus on future attention in this direction. Also considering the 3D advection-diffusion models.

Acknowledgements

The first author would like to thank PROMEC/UFRGS and CNPq for the master's scholarship he received during the production of this paper.The co-authors also thank the CNPq for partial financial support of this work.

References

[1] Roache, P., 1972. *Computational Fluid Dynamics*. Hermosa Publishers.

[2] Cunha, C., Carrer, J., Oliveira, M., & Costa, V., 2016. A study concerning the solution of advection–diffusion problems by the boundary element method. *Engineering Analysis with Boundary Elements*, vol. 65, pp. 79 – 94.

[3] Ikeuchi, M. & Onishi, K., 1983. Boundary element solutions to steady convective diffusion equations. *Applied Mathematical Modelling*, vol. 7, n. 2, pp. 115 – 118.

[4] Qiu, Z. H., Wrobel, L. C., & Power, H., 1998. Numerical solution of convection–diffusion problems at high péclet number using boundary elements. *International Journal for Numerical Methods in Engineering*, vol. 41, n. 5, pp. 899–914.

[5] Wrobel, L. & DeFigueiredo, D., 1991. A dual reciprocity boundary element formulation for convection-diffusion problems with variable velocity fields. *Engineering Analysis with Boundary Elements*, vol. 8, n. 6, pp. 312 – 319.

[6] Brebbia, C., Telles, J., & Wrobel, L., 1984. *Boundary Element Techniques*. Springer-Verlag.

[7] Telles, J. C. F., 1987. A self-adaptive co-ordinate transformation for efficient numerical evaluation of general boundary element integrals. *International Journal for Numerical Methods in Engineering*, vol. 24, n. 5, pp. 959–973.

[8] Brebbia, C. & Dominguez, J., 1992. *Boundary elements, an introductory course*. WIT Press.

[9] Elliott, D., Holladay, C., Barchet, W., Foote, H., & Sandusky, W., 1987. Wind energy resource atlas of the United States.

[10] World Meteorological Organization, 2014. *Guide to Meteorological Instruments and Methods of Observation*. WMO.